HAMAMATSU

PHOTON IS OUR BUSINESS

NEWS 2023 01

COVER STORY | PAGE 3

Hamamatsu Photonics Has Developed a New Spectrometer with Ultra-High Dynamic Range

CONTENT

Hamamatsu News – now also online:
www.hamamatsu-news.com

Hamamatsu Photonics Has Developed a New Spectrometer with Ultra-High Dynamic Range

By leveraging our unique opto-semiconductor design technology and software technology, we have succeeded in developing a new spectrometer having an extremely high dynamic range of 2,500,000 to 1 in the spectral range from 200 nm to 900 nm that allows simultaneous measurement of both strong and weak signals. This high dynamic range spectrometer called "OPAL-Luxe™ C16736-01" is the top-end model among our spectrometer lineup.

Incorporating the OPAL-Luxe™ into component analyzers that utilize light absorption properties of substances in the ultraviolet to near-infrared region, it will allow simultaneous analysis of the various components within a sample. This includes components in large quantities absorbing large amounts of light and components in small quantities absorbing small amounts of light. This increases component analysis efficiency in the quality control of chemicals by detecting the trace amounts of impurities in substances without having to repeat measurements. The OPAL-Luxe™ will also help make further progress in plasma application research since it can analyze plasma emissions with high accuracy.

The new OPAL-Luxe™ was launched at the SPIE Photonics West 2023 exhibition in San Francisco, California, USA, 31st January to 2nd February 2023.

Mr. Tadashi Maruno Announced as Representative Director and President

Mr. Tadashi Maruno was named as Representative Director and President during the 75th ordinary meeting of Hamamatsu Photonics K.K. in mid-December 2022.

Mr. Tadashi Maruno has been working with Hamamatsu Photonics for forty years. Prior to this role, he has been Representative Director and Senior Managing Executive Officer. He also worked as General Manager (2014) and then later as Division Director (2017) of the Systems Division which includes all of the Manufacturing and Semiconductor support systems, Photometry systems, and Life science & medical systems.

"We are looking forward to working with Mr. Tadashi Maruno and the new Management team as they navigate us toward further success!"

Max Skoglund, Hamamatsu Photonics Europe Managing Director

Hamamatsu's previous Representative Director and President for 13 years, Mr. Akira Hiruma is now the Representative Director and Chairman.

Hamamatsu Photonics and B-PHOT VUB Renew Their Collaboration to Pursue Breakthroughs in Photonics Research and Innovation Across Europe

On December 5th, 2022, at the occasion of the Belgian Economic Mission to Japan in Tokyo, the largest Belgian trade mission to Japan to date, Hamamatsu Photonics, represented by Akira Hiruma (President Chief Executive Officer*) and B-PHOT VUB (Brussels Photonics VUB) represented by Professor Hugo Thienpont, renewed their original agreement to strengthen collaborative endeavors in photonics research and innovation.

First chaired in November 2019, Hamamatsu Photonics entered into a partnership with B-PHOT VUB, the photonics research group of the Vrije Universiteit Brussel, Belgium, by creating HAPI (Hamamatsu Applied Photonics Innovation).

Both parties signed to continue their activities with an increased funding commitment from Hamamatsu to support the development of photonics technology for its great economic and societal impact. This event was the ideal vehicle to intensify mutual collaboration between both Hamamatsu Photonics experts and B-PHOT VUB researchers, to exchange information on the latest research breakthroughs in the domain of photonics and their potential applications, and to further explore opportunities for a fruitful long-term partnership.

Also present during the Belgian Economic Mission to Japan, was her Royal Highness of Belgium, Princess Astrid, and the Prime Minister of Japan, Mr. Fumio Kishida.

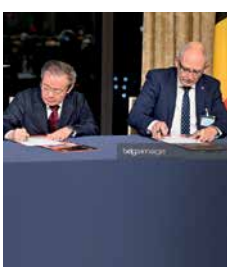

Picture on the left: Joy Donné (CEO Flanders Investment & Trade), Hugo Thienpont, Jan Jambon (Minister-President of Flanders), Akira Hiruma (former CEO Hamamatsu Photonics), Yasutomo Suzuki (Hamamatsu City Mayor).

Center picture and right picture: Mr. Hiruma, Hugo Thienpont. Copyright BELGA

*Since January 2023, Akira Hiruma is the Representative Director and Chairman of Hamamatsu Photonics. The Representative Director and President Chief Executive Officer is now Tadashi Maruno.

SPIE. PHOTONICS WEST

Hamamatsu's Light Shines at Photonics West & BiOS Expo

January saw Hamamatsu Photonics return to the combined annual Photonics West and BiOS Expo exhibitions in California. Photonics West is one of the leading global exhibitions in its field, created as a single place where delegates from around the world can find the best components, solutions, and systems in photonics, quantum, optoelectronics, and laser technologies. The sister BiOS Expo is a key place for healthcare and biomedical industries to discover the ideal biomedical optics and bio-photonics solutions for their needs.

We were delighted to participate in what was a particularly successful and well-attended event with over 22,000 registered visitors, a vast improvement from last year's 10,000 visitors, over 1,400 exhibitors, and more than 4,500 technical presentations, making a return to pre-COVID-19 attendance levels for delegates and exhibitors alike. It was a pleasure to engage with our customers from across the world in person, and in some cases for the first time since the COVID-19 restrictions began.

Hamamatsu Photonics took this opportunity to demonstrate a host of new developments, technologies, and solutions designed for biomedical research, healthcare, and the industrial and environmental markets. Our colleagues shared their expertise through technical talks and conference presentations on current research that gave key insights into their respective industries while automotive LiDAR and our advanced quantum imaging technologies gained the most attention at the Photonics West stand. We were pleased to experience a constant stream of visitors to Hamamatsu's booth due to the exciting new and ground-breaking products on display including the OPAL-Luxe™ High dynamic range spectrometer, the diffuse reflection light source, and the InAsSb photovoltaic detector with its preamplifier as well as our award-winning ORCA-Quest camera for quantitative imaging.

Hamamatsu Ventures also made a positive impact as a lead sponsor with the Start-up Challenge Pitch competition. Entrepreneurs in young optics and photonics businesses eagerly vied for the $10,000 prize on offer hoping to win the place for the most promising technology in the healthcare and deep tech industries.

Discover more of what Hamamatsu Photonics had to offer at the Photonics West and BiOS Expo exhibitions on our Photonics West site: **pw.hamamatsu.com**

Series Mitochondria

The Little Giants Inside Cells That Maintain Life and Health

Commentary:
Hideo Tsukada, Ph.D.,
Central Research Laboratory, Hamamatsu Photonics K.K.

Part 3

Detecting changes in mitochondrial functions of brains with Alzheimer's disease using PET

In Part 2 of this series, we described designing a PET (Positron Emission Tomography) probe essential for making non-invasive measurements of mitochondrial functions, in the brain of middle-aged animals and animals with Alzheimer's disease. The results clearly demonstrated its effectiveness. Now in Part 3, we will further review this previous research and also present its effect on human patients.

Two blueprints for mitochondria

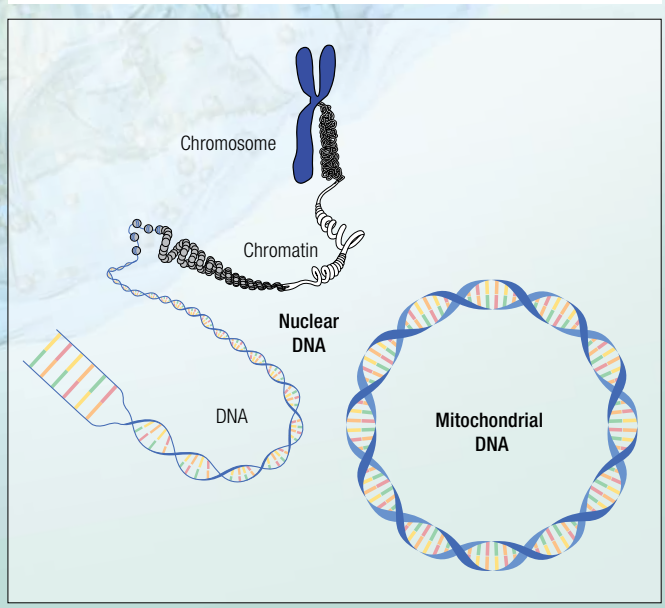

Figure 1: DNA is a blueprint of proteins that make up mitochondria and is present in two locations in a cell as the mitochondria and nucleus. Unlike nuclear DNA with a chromatin structure in which DNA is wrapped around proteins, ring-shaped mitochondrial DNA is naked so to speak and mutates more easily due to external damage.

Measuring mitochondrial functions in aged monkey brains

The "mitochondrial theory of aging" is one hypothesis for explaining aging. Oxidative phosphorylation in mitochondria produces ATP (Adenosine Triphosphate) which is an energy source essential for maintaining cell activity, but this process produces harmful by-products called ROS (Reactive Oxygen Species) at the same time. When the antioxidant function declines with age, it becomes difficult to eliminate ROS and this excessive ROS damages the mitochondrion itself. These damaged mitochondria then produce more ROS, creating a vicious cycle that further magnifies the damage. This ROS-triggered oxidative stress can damage the DNA, lipids and proteins that make up cells. In particular for mitochondrial DNA (Figure 1) as it does not have a chromatin structure, it is more likely to suffer damage compared to nuclear DNA that has one. Mitochondrial DNA also has poor self-repair capability so that DNA damage associated with aging continues to accumulate. These factors lead to a gradual decline in mitochondrial functions which lowers the ATP production rate below the threshold level and causes dysfunctional cells to accumulate due to lack of energy. Moreover, inflammatory cells induced by these damaged cells also secrete ROS and other various inflammatory substances that fuel this vicious cycle, resulting in a gradual loss of homeostasis in an organism. This hypothesis of aging is known as the "mitochondrial theory of aging." It suggests that neurodegenerative diseases such as Alzheimer's disease and Parkinson's disease result from neuronal cell damage enhanced by these aging factors as well as other causes specific to each disease, such as deposition of abnormal proteins.

To confirm the "mitochondrial theory of aging" hypothesis, we conducted research on how aging affects mitochondrial complex-I (MC-I) activity by examining the brains of rhesus monkeys *(Macaca mulatta)*. In PET imaging of laboratory animals, anesthesia is routinely

Decrease in MC-I activity in the brains of conscious monkeys measured by PET imaging

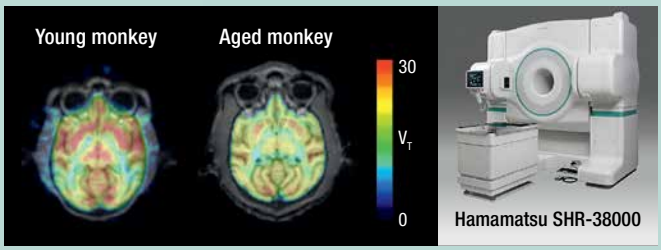

Figure 2: Using the PET camera system for laboratory animals that measures the brain function of a conscious monkey sitting in a chair by tiling the scanning gantry, we measured the MC-I activity in the brain of a young and aged rhesus monkeys using [^{18}F]FDG-EF. The results detected in the brain of the aged monkey show a decrease in MC-I activity.

used to immobilize the animal during measurement. However, the effects these anesthetics render on the brain functions and on the in vivo dynamics of the PET probes cannot be ignored (Reference 1). So we used a PET camera system (Hamamatsu SHR-38000 shown in Figure 2) capable of measuring the brain functions of conscious monkeys along with [^{18}F]BCPP-EF which is a PET probe for MC-I measurement. Then, we compared a young monkey, around 5 years old (equivalent to 20 human years) with an aged monkey of more than 20 years (equivalent to 80 human years). The results showed a significant decrease in MC-I activity in the brain with aging (Figure 2) (Reference 2). Up to now, it has been suggested that MC-I activity decreases with aging as found through analysis of post-mortem brain tissue samples removed during brain tumor surgery. Our research is the first in the world to detect a decrease in MC-I activity in the brains of living primates.

We already reported an age-related decrease in the glucose metabolic rate throughout the brains of rhesus monkeys by conducting PET imaging research using [^{18}F]FDG (Fluoro-2-deoxy-D-glucose) (Reference 3). While MC-I activity in the cerebral cortex measured with [^{18}F]FDG-EF decreased by an average of 36% with aging, the decrease in glucose metabolic rate measured with [^{18}F]FDG remained at 27% on average. This difference between these two parameters in the level of decrease is assumed to reflect the uptake of [^{18}F]FDG not only into normal neurons but also into inflammatory cells (microglia) activated in response to age-damaged neurons (Reference 4), (also described in Part 2).

Effects of Aβ protein deposition on inflammation and MC-I activity

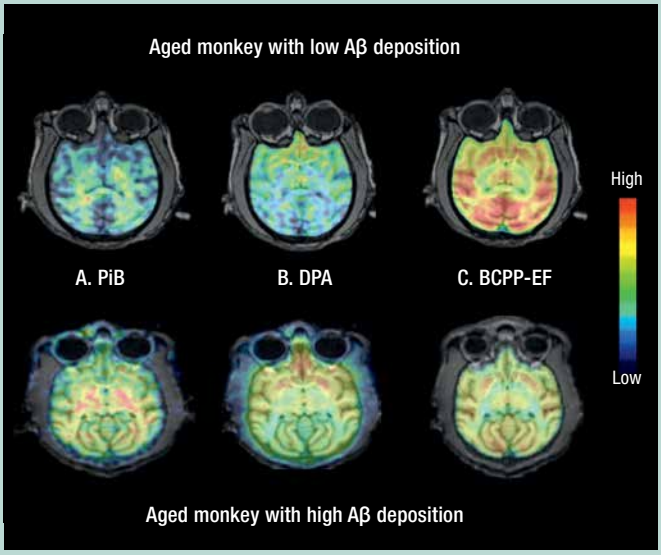

Figure 3: Among aged rhesus monkeys, the monkey with high Aβ protein deposition in the brain (A. [^{11}C]PiB) showed more inflammation (B. [^{11}C]DPA-713) and lower MC-I activity (C. [^{18}F]BCPP-EF) compared to the monkey with low Aβ protein deposition in the brain.

Aβ protein deposition and MC-I activity in aged monkey brains

In basic research on neurodegenerative diseases associated with aging, a common approach is using senescence-accelerated mice or genetically modified mice (transgenic mice) with forced expression of pathogenic abnormal proteins in their brains. Using these mice to conduct PET research utilizing [^{18}F]BCPP-EF, we proved that the decrease of the MC-I function stems from Aβ (Amyloid-β) protein depositions in the brain of senescence-accelerated mice (Reference 5) and from Tau protein deposition in the brain of transgenic mice (Reference 6).

However, rodent's (mice and rats) pathological models are often emphasized by focusing only on particular aspects of human pathological conditions and do not always reflect the complexity of human diseases. Meanwhile, over many years, we have conducted PET research on age-related changes in monkey brain functions (References 3 and 7) and obtained results showing that "some monkeys showed high Aβ protein deposition in their brains with aging" (Reference 8). Although further discussion is needed to conclude that "high Aβ protein deposition in the brain is the Alzheimer's disease model of monkeys," we examined the relationship between Aβ protein deposition and mitochondrial functions in the brain of rhesus monkeys. After a detailed re-analysis of the results obtained from the previously mentioned young and aged monkeys (Reference 2), we found that individual differences in MC-I activity in the brain of aged monkeys were greater than those in young monkeys. To find out the reason for this, we focused on individual differences in Aβ protein deposition in the brains of aged monkeys. Our findings indicated that the MC-I activity (measured with [^{18}F]BCPP-EF) of the monkey with high Aβ protein deposition (measured with [^{11}C]PiB) in their cerebral cortex was lower than that of the monkey with low Aβ protein deposition (A and C in Figure 3) (Reference 9).

On the other hand, the monkey with high Aβ protein deposition did not always show a decreased accumulation of [^{18}F]FDG which reflects the glucose metabolic rate. Since the monkey with high Aβ protein deposition in the brain showed a high level of intracerebral inflammation, measured with [^{11}C]PA-713 (B in Figure 3), the activated microglia that accumulated and proliferated, at the impacted site in response to damage, had a large uptake of [^{18}F]FDG. This implies that the reduced uptake of [^{18}F]FDG caused by Aβ-protein-induced neuronal damage might not have been detected correctly. This conclusion of "detecting neuropathy with [^{18}F]FDG is difficult because of intracerebral inflammation that is induced as the amount of Aβ protein deposition increases" was confirmed in several papers on transgenic mice (References 10 and 11).

Assessment of MC-I function in the human brain

In 2015 when we started clinical PET research on human patients while evaluating the novel PET probe [^{18}F]BCPP-EF for monkey brains, we received an offer from Invicro LLC, United Kingdom for a collaborative research on the clinical assessment of [^{18}F]BCPP-EF. Invicro, a biotechnology business supports drug development by harnessing clinical PET imaging technology. They believed that a new concept in PET probes other than [^{18}F]FDG would prove essential for supporting development of therapeutic agents for Alzheimer's disease and other neurodegenerative disorders. After a literature search, they narrowed their focus down to three types of PET probes including the [^{18}F]BCPP-EF that we had developed. This clinical assessment was first initiated as a consortium (MIND-MAPS project) led by Invicro and our company with participation from universities in the UK. But shortly after, several major US and European pharmaceutical companies, aligned with the purpose of the project also joined in. So this clinical assessment of novel PET probes transformed into a global consortium from Japan, Europe and the US, including representatives from the pharmaceutical industry.

Safety and exposure dose assessments in rodents are essential and mandatory for applying novel PET probes to clinical research on human subjects. Since we had envisioned to conduct research on potential clinical applications, we already possessed relevant data. This helped to facilitate a smooth start with Invicro. To see if the results we obtained with monkeys could be reproduced in measurements on humans, we calculated MC-I activity in healthy subjects using the same method and obtained results that well reflected the mitochondrial activity in the brain which had been found in human postmortem brains.

Reproducibility of [^{18}F]BCPP-EF measurements on healthy subjects and effect from aging

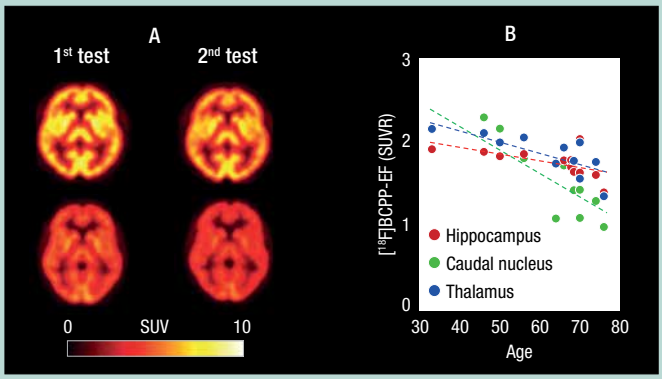

Figure 4: (A) Results of repeated measurements on healthy subjects using the [^{18}F] BCPP-EF showed high reproducibility for both subjects with high MC-I activity (upper row) and with low MC-I activity (lower row). (B) Decrease in MC-I activity was observed in various regions of the brain due to aging.

Reproducibility of repeated measurements on the same person is important for determining the therapeutic efficacy. The range of its variability remained below 7% regardless of the level of MC-I activity in each individual, proving high reproducibility in PET measurements on humans (A in Figure 4) (Reference 12). We also evaluated physiological age-related changes in MC-I activity in the brain and were able to detect significant reductions in each region of the human brain just as with monkey brains (B in Figure 4) (Reference 13).

Assessment of MC-I activity in the brain of Alzheimer's disease patients

In the course of this global clinical PET research, at the time when we became much more confident of the usefulness of MC-I measurements using [^{18}F]BCPP-EF in the human brain, we were able to begin clinical PET research with the Hamamatsu University School of Medicine in order to assess MC-I activity in the brains of Alzheimer's disease patients. We found that patients with early Alzheimer's disease have significantly reduced MC-I activity in the parahippocampal gyrus which plays an important role in memory, compared to healthy older adults of the same age (A in Figure 5) (Reference 14). MC-I activity in the entorhinal cortex (including the parahippocampal gyrus) of the medial temporal lobe in a brain region impaired at an early stage of onset (Braak stage I-II) showed a significant positive correlation with the index of memory ability (A in Figure 6) (References 15 and 16).

Furthermore, in the MIND-MAPS project, after repeatedly measuring the same patient over a period of 1.5 to 2 years, we observed a decrease in MC-I activity that reflected a cognitive decline associated with the progression of Alzheimer's disease (C in Figure 6) (Reference 17). On the other hand, when assessing the glucose metabolic rate using [^{18}F]FDG, no changes in [^{18}F]FDG accumulation were detected in the parahippocampal gyrus between healthy subjects and Alzheimer's disease patients (C in Figure 5) (Reference 14). One possible reason for this is that mitochondrial dysfunction may precede the abnormal glucose metabolism in the early neurological damage from Alzheimer's disease. The damage to the neurons might also be detected incorrectly because microglia activated in response to the accumulate damage at the impacted site may be causing uptake of [^{18}F]FDG (References 9 to 11).

Besides Aβ protein, Tau protein is considered a causative agent of Alzheimer's disease. As described earlier, in the hippocampus of transgenic mice we not only found Tau protein deposition, measured with [^{11}C]PBB3, but also that inflammation and brain atrophy were associated with a decrease in MC-I activity measured with

[^{18}F]BCPP-EF (Reference 6). In the parahippocampal gyrus where a decrease in MC-I activity occurred in patients with early Alzheimer's disease (A in Figure 5), abnormal deposition of Tau protein was observed earlier than in any other brain regions (B in Figure 5), indicating a significant negative correlation between the two PET probes (B in Figure 6). At this point, a large amount of Aβ protein had already been deposited in the entire cerebral cortex (Reference 15). These results suggest that the gradual deposition of Aβ protein in the entire cerebral cortex was initiated well before the onset of Alzheimer's disease and that the neural dysfunction induced by abnormal deposition of Tau protein in the parahippocampal gyrus and mitochondrial dysfunction at an early stage of disease led to impairment of short-term memory ability.

Although the spatio-temporal relationship between Aβ protein, Tau protein and mitochondria in Alzheimer's disease still remains unclear, Melov et al. examined the offspring of a mouse with reduced mitochondrial antioxidant activity alongside another with abnormal deposition of Aβ protein. They then suggested the hypothesis that Aβ protein (probably the most toxic oligomeric form) generated in neurons causes mitochondrial dysfunction and generates ROS, and the activated microglia induced by neuropathy also generates ROS. The subsequent production of Aβ protein promoted by these increased ROS may further increase ROS-induced oxidative stress, leading to abnormal deposition of Tau and neuropathy in the hippocampus. The results we presented here from the series of clinical PET measurements support this hypothesis.

In Part 4 which will be the final of this series, we will present the usefulness of MC-I measurement by PET imaging in areas other than the brain since mitochondria are found in almost every cell in the body.

PET imaging of the brain of Alzheimer's disease patient

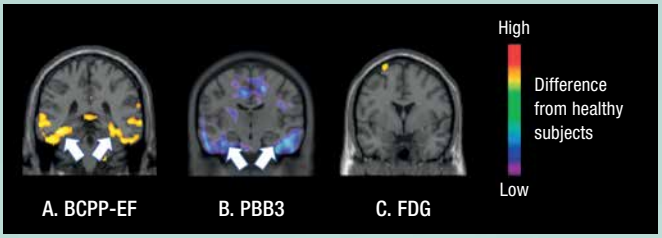

Figure 5: In the brains of patients with early-stage Alzheimer's disease, MC-I activity (A. [^{18}F]BCPP-EF) was reduced in the parahippocampal gyrus (indicated by arrows) compared to healthy subjects, which is consistent with early high deposition sites of Tau protein (B. [^{11}C]PBB3). In contrast, glucose metabolism (C. [^{18}F]FDG) did not show a decrease in any region including the parahippocampal gyrus.

Association between MC-I activity, cognitive function, and Tau deposition in the brains of Alzheimer's disease patients

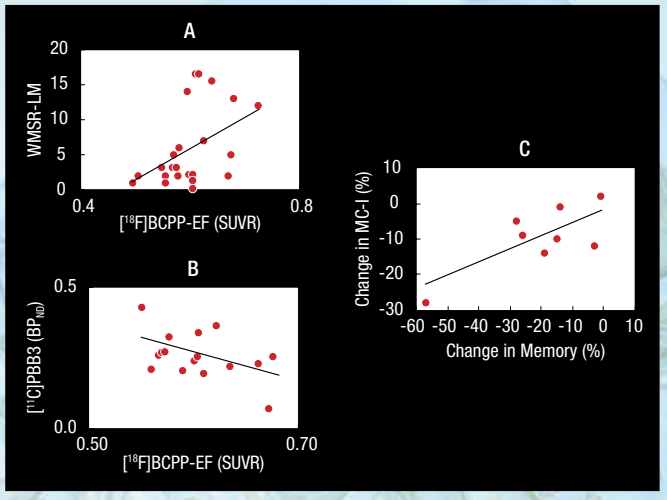

Figure 6: In the brain regions first affected in patients with early Alzheimer's disease, MC-I activity ([^{18}F]BCPP-EF) and memory ability (WMSR-LM) were positively correlated (A), while MC-I activity and Tau deposition ([^{11}C]PiB) were negatively correlated (B). A positive correlation was found between MC-I activity and memory ability that declined over 18 months to 2 years (C).

References

1. Tsukada H. PET Imaging of Dopaminergic Function in Non-Human Primates. In Serotonin and Dopamine Receptors: Functions, Synthesis and Health Effects, Munoz M and Mckinney M (Eds). Nova Science Publishers, New York, pp.45-78 (2018).
2. Tsukada H, et al. Evaluation of ^{18}F-BCPP-EF for mitochondrial complex I imaging in conscious monkey brain using PET. Eur J Nucl Med Mol Imaging. 2014;41:755-763.
3. Noda A, et al. Determination of kinetic rate constants for FDG and partition coefficient of water in conscious macaque and alterations in aging or anesthesia examined on parametric images with an anatomic standardization technique. J Cereb Blood Flow Metab. 2003;23:1441-1447.
4. Kumar A, et al. Evaluation of age-related changes in translocator protein (TSPO) in human brain using ^{11}C-[R]-PK11195 PET. J Neuroinflammation. 2012;9:232.
5. Yamagishi S, et al. In vivo alterations of mitochondrial activity and amyloidosis in early-stage senescence -accelerated mice: a positron emission tomography study. J Neuroinflammation. 2021;18:288.
6. Barron AM, et al. In vivo PET imaging of mitochondrial abnormalities in a mouse model of tauopathy. Neurobiol Age. 2020;94:140-148.
7. Tsukada H. PET Imaging Research on Brain Aging in Non-human Primates. In Horizons in Neuroscience Research 27, Costa A and Villalba E (Eds). Nova Science Publishers. New York. pp.149-176 (2016).
8. Noda A, et al. Amyloid imaging in aged and young macaques with [^{11}C]PIB and [^{18}F]FDDNP. Synapse. 2008;62:472-475.
9. Tsukada H, et al. Comparing amyloid-β deposition, neuroinflammation, glucose metabolism, and mitochondrial complex I activity in brain: A PET study in aged monkeys. Eur J Nucl Med Mol Imaging. 2014;41:2127-2136.
10. Brendel M, et al., Glial activation and glucose Metabolism in a transgenic amyloid mouse model: A triple-tracer PET study. J Nucl Med. 2016;57:954-960.
11. Xiang X, et al. Microglial activation states drive glucose uptake and FDG-PET alterations in neurodegenerative diseases. Sci Transl Med. 2021;13:eabe5640.
12. Mansur A, et al., Test-retest variability and reference region based quantification of ^{18}F-BCPP-EF for imaging mitochondrial complex I in the human brain. J Cereb Blood Flow Metab. 2021;41:771-779.
13. Mansur A, et al. Characterization of 3 PET tracers for quantification of mitochondrial and synaptic function in healthy human brain: ^{18}F-BCPP-EF, ^{11}C-SA-4503, ^{11}C-UCB-J. J Nucl Med. 2020;61:96-103.
14. Terada T, et al., In vivo mitochondrial and glycolytic impairments in Alzheimer's disease. Neurology. 2020; 94:e1592-e1604.
15. Terada T, et al., Mitochondrial complex I abnormalities is associated with tau and clinical symptoms in mild Alzheimer's disease. Mol Neurodegener. 2021;16:28.
16. Terada T, et al., Mitochondrial complex-I abnormalities underlie neurodegeneration and cognitive decline in Alzheimer's disease. Eur J Neurol. 2022;29:1324 -1334.
17. Venkataraman AV, et al. Widespread cell stress and mitochondrial dysfunction in early Alzheimer's Disease. Sci Trans Med. 2022;14:eabk1051.
18. Melov S, et al. Mitochondrial oxidative stress causes hyperphosphorylation of tau. PLoS ONE. 2007;2:e536.

Image Sensor Modules C15853-01/-02

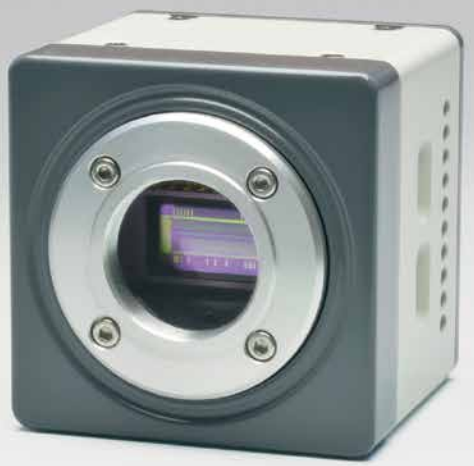

Specifications

Parameter		C15853-01	C15853-02	Unit
A/D resolution		16		bit
Interface		USB 3.1 Gen1		–
Dimensions (W × H × D)*		60 × 60 × 54		mm
Built-in sensor	Type No.	InGaAs linear image sensor G14714-512DE	InGaAs linera image sensor G14714-1024DK	–
	Spectral response range	0.95 to 1.7		µm
	Number of effective pixels	512	1024	pixels
	Pixel size (H × V)	25 × 25	12.5 × 12.5	µm
	Image size	12.8 × 0.025	12.8 × 0.0125	mm

* Excluding protrusions

Block diagram

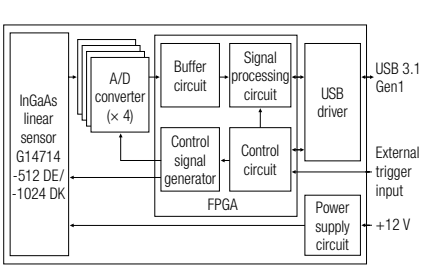

Application example: grain sorter

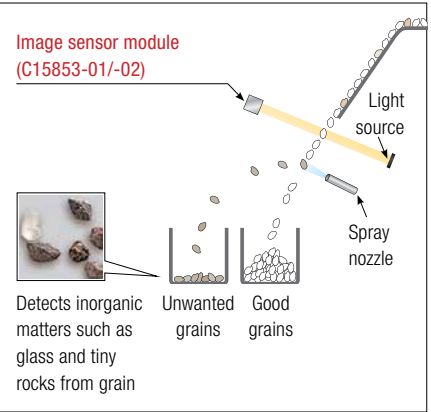

Built-in InGaAs Linear Image Sensor with Near Infrared Sensitivity, High-speed Line Rate Realized

This image sensor module is equipped with an InGaAs linear image sensor (G14714-512DE/-1024DK). This product has sensitivity in the near infrared region of 0.95 to 1.7 µm, and is capable of readout at a high-speed line rate of 40 klines/s. It transfers the acquired image signal to a PC via a USB 3.1 Gen1 interface. The SMA connector for external trigger input is attached to the main body, making it possible to synchronize an operation with external devices. Also, C-mount compatible lens can be used.

Features

- High-speed line rate: 40 klines/s max.
- Digital output
  A/D resolution: 16-bit
- Interface: USB 3.1 Gen1
- Non-cooled operation
- Compact module

Applications

- Foreign object detection
- Farm product inspection
- Spectrophotometry
  (built-in spectrometer)

NEW OPTO-SEMICONDUCTOR PRODUCTS

Distance Image Sensors S16443-01WT, S16444-01WT

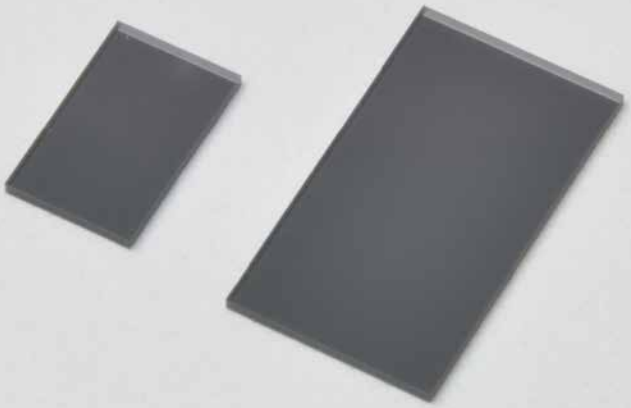

Imaging examples

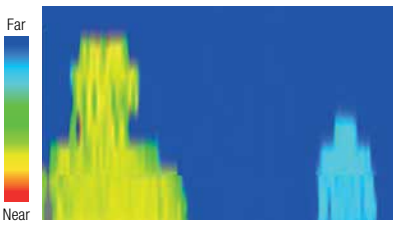

Using S16443-01WT (distance image)

Commercial camera (visible image)

Specifications

Parameter	NEW S16443-01WT	NEW S16444-01WT	S15452-01WT	S15453-01WT	S15454-01WT
Photo					
Type	Area sensor		Linear sensor		Area sensor
Number of effective pixels	128 (H) × 8 (V)	320 (H) × 20 (V)	64	256	96 (H) × 72 (V)
Pixel pitch (μm)	20 (H), 201.5 (V)		20		50 (H, V)
Image size [H × V (mm)]	2.56 × 1.612	6.4 × 4.03	1.28 × 0.05	5.12 × 0.05	4.8 × 3.6
Spectral response range (nm)	500 to 1100				

TOF (time of flight) Sensors for Image Monitors Which Require Privacy Concern

Security cameras are intended to capture images of suspicious persons and activities, so they must be able to capture high resolution images. However, in situations such as 'status monitoring' of the number of people passing through ticket gates and automatic doors, or 'safety monitoring' of elderly people in bedrooms or bathrooms, consideration must be made for privacy, by using low resolution monitoring. We have newly added two distance image sensor products (128 × 8 pixels, 320 × 20 pixels) to our lineup of products that can be used in such situations. A distance image sensor measures the distance to objects, and it can image the silhouette of the object from the distance information it acquires.

Features

- 2 new types of different number of pixels (128 × 8 pixels, 320 × 20 pixels)
- Higher sensitivity in the near infrared region (compared to previous products)
- Improved tolerance to background light (compared to previous products)
- Compact chip size package (CSP) type

Related products

Evaluation kit
An evaluation kit is available for the distance image sensors (with the sensor). Contact us for detailed information.

H15472-01

ASIC for distance image sensors
There are built-in circuits (driver circuit, A/D converter), etc. for I/O of distance image sensors. It outputs data in such a format as to be directly connected to a microcontroller. It helps to make devices smaller and lighter compared to the case where a general-purpose IC is used.

CERARION® Electron Multiplier R14747-80

Specifications

Parameter	Specifications	Unit
Gain (typ.)*1, 2	1.0×10^7	–
Dark count (max)*1	2.0	s^{-1}
Dark current (typ.)*1	1.0	pA
Effective area	ϕ11	mm
Rise time (typ.)*1,2	2.1	ns

*1 CEM In supply voltage: -2100 V
CEM Out supply voltage: -100 V
Conversion dynode supply voltage: -10 kV
Operating pressure: 1.0×10^{-4} Pa
*2 Input ion: *m/z* 18

Gain characteristics

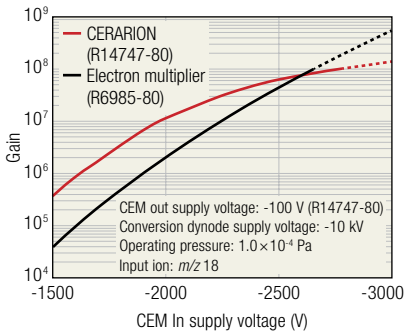

Lead-free Channel Electron Multiplier with Conversion Dynode

The R14747-80 is a lead-free channel electron multiplier (CERARION®) with a conversion dynode. The shape, number of channels, and signal readout method can be customized according to equipment requirement.

The conversion dynode allows the CERARION® to measure even heavy ions. Positive and negative ions can be rapidly measured by switching the polarity of the voltage to the conversion dynode.

Application

- Mass spectrometers (Ion trap MS, QMS)

T-SMILS Laser Heating System
L15570-111/-211/-311

Specifications

Type.no		L15570-111	L15570-211	L15570-311
Light source (SPOLD® LD irradiation light source)	Laser output power	30 W (min)	75 W (min)	200 W (min)
	Oscillation type	CW		
	Peak emission wavelength (25 °C)	940 nm ± 20 nm		
	Cooling method	Air cooling		Water cooling
Irradiation unit	Spot size	ϕ0.8 mm to ϕ6.4 mm (depends on irradiation optics)		
Protocol	Communication standard	Ethernet: TCP/IP		

Feedback function

Feedback function enables proper heating control at corners for higher precision processing. Target: Plastic (ABS) welding

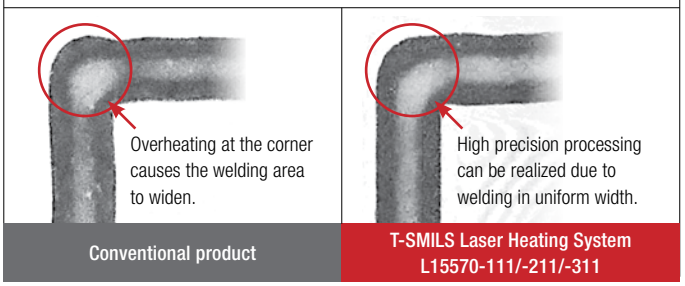

Laser Heating System Equipped with a Temperature Measurement at the Processing Point and Feedback Function

This is a laser heating system equipped with a temperature measurement function. Since the processing state depends on the temperature at the processing point, various laser heating processes, including plastic welding can be carried out with high precision by implementing the temperature measurement function. PC sample app can be used to set the laser specifications for easier conditioning of the laser irradiation. It also supports external control, enabling mass production such as integration into equipment.

Features

- Equipped with a laser output feedback function that enables processing at a constant temperature
- Laser heating while measuring the precise temperature at the processing point (2-color method is applied)
- Uniform beam profile (top-hat shape)
- Easy connection with external equipment (robotics, PCs, etc.), high-FA compatibility, best suited for Industry 4.0, etc.
- Sample app available for linkage with PC

Applications

- Conditioning for various laser processing
  - Plastic welding
  - Soldering
  - Thermal curing of adhesive
  - Sintering of metal nanoinks
  - Waterproof seal
  - Hardening of metal

Laser Heating System
L16470-111/-241, L16480-112/-344, L16490-343

Laser Heating System Designed For Specific Heating Processing

This laser heating system can optimally combine a light source, fiber, and lens to suit applications such as soldering, heat curing of adhesives, and plastic welding by laser. The temperature monitoring function at the processing point enables real-time 'visualization' of laser processing.

Differences from the previous product

Previously, users had to chose necessary products and accessories from the product specifications. However, the selection of the model is made easier by setting the light source and optical system to suit the processing application.

Features

- Energy and space saving
- No individual difference
- Ideal for mass production processes
- Processing temperature monitoring function

Applications

- Soldering
  - Small electronic components
  - Motor parts
  - Glass and ceramic packages
- Plastic welding
  - Automotive parts
  - Medical instruments
  - Electronic components
- Thermal curing of adhesive
  - Plastics, Metals & Glasses

Application examples

Soldering (L16470-111/-241)

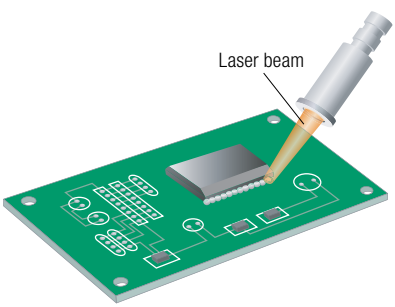

Thermal curing of adhiesive (L16480-112/-344)

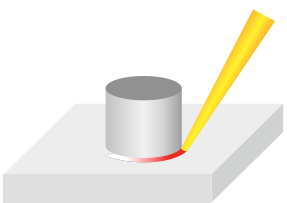

Plastic welding (L16490-343)

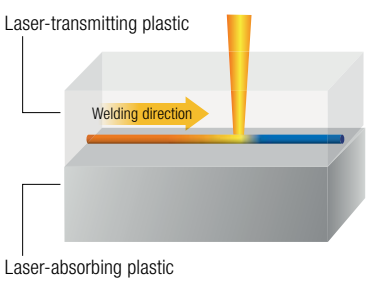

Hamamatsu Photonics K.K. Sales Offices

Japan:
HAMAMATSU PHOTONICS K.K.
325-6, Sunayama-cho, Naka-ku,
Hamamatsu City, Shizuoka Pref. 430-8587, Japan
Telephone: (81)53-452-2141, Fax: (81)53-456-7889
E-mail: intl-div@hq.hpk.co.jp

China:
HAMAMATSU PHOTONICS (CHINA) CO., LTD.
Main Office
1201, Tower B, Jiaming Center, 27 Dongsanhuan Beilu,
Chaoyang District, 100020 Beijing, P.R. China
Telephone: (86)10-6586-6006, Fax: (86)10-6586-2866
E-mail: hpc@hamamatsu.com.cn

Shanghai Branch
4905 Wheelock Square, 1717 Nanjing Road West,
Jingan District, 200040 Shanghai, P.R. China
Telephone: (86)21-6089-7018, Fax: (86)21-6089-7017
E-mail: hpcsh@hamamatsu.com.cn

Shenzhen Branch
14F China Merchants Tower 1#, No. 1166 Wanghai Road,
Shekou, Nanshan District, Shenzhen, P.R. China
Telephone: (86)755-2165-9058, Fax: (86)755-2165-9056
E-mail: hpcsz@hamamatsu.com.cn

Wuhan Branch
Room 1005 Fanyue City T2 Building, No. 19 Guanshan Avenue,
East Lake High-tech District, Wuhan 430075, Hubei, P.R. China
Telephone: (86)27-5953-8219
E-mail: hpcwh@hamamatsu.com.cn

Taiwan:
HAMAMATSU PHOTONICS TAIWAN CO., LTD.
Main Office
8F-3, No.158, Section 2, Gongdao 5th Road,
East District, Hsinchu, 300, Taiwan R.O.C.
Telephone: (886)3-659-0080, Fax: (886)3-659-0081
E-mail: info@hamamatsu.com.tw

U.S.A.:
HAMAMATSU CORPORATION
Main Office
360 Foothill Road, Bridgewater, NJ 08807, U.S.A.
Telephone: (1)908-231-0960, Fax: (1)908-231-1218

California Office
2875 Moorpark Ave., San Jose, CA 95128, U.S.A.
Telephone: (1)408-261-2022, Fax: (1)408-261-2522

ENERGETIQ TECHNOLOGY, INC.
205 Lowell Street, Wilmington, MA 01887, U.S.A.
Telephone: (1)781-939-0763, Fax: (1)781-939-0769
E-mail: info@energetiq.com

Germany, The Netherlands, Poland, Denmark, Israel:
HAMAMATSU PHOTONICS DEUTSCHLAND GMBH
Main Office
Arzbergerstr. 10, 82211 Herrsching am Ammersee, Germany
Telephone: (49)8152-375-0, Fax: (49)8152-265-8
E-mail: info@hamamatsu.de

Netherlands Office
Transistorstraat 7, 1322 CJ Almere, The Netherlands
Telephone: (31)36-5405384, Fax: (31)36-5244948
E-mail: info@hamamatsu.nl

Poland Office
10 Ciolka Street, 126-127 01-402 Warsaw, Poland
Telephone: (48)22-646-0016, Fax: (48)22-646-0018
E-mail: poland@hamamatsu.de

Danish Office
Lautruphøj 1-3, 2750 Ballerup, Denmark
Telephone: (45)8874 5312
E-mail: info@hamamatsu.dk

Israel Office (HAMAMATSU PHOTONICS ISRAEL LTD.)
Ha-Menom 10 st., third floor, 4672561 Herzliya, Israel
E-mail: Info@hamamatsu.co.il

France, Switzerland, Belgium, Spain:
HAMAMATSU PHOTONICS FRANCE S.A.R.L.
Main Office
19 Rue du Saule Trapu, Parc du Moulin de Massy,
91882 Massy Cedex, France
Telephone: (33)1 69 53 71 00, Fax: (33)1 69 53 71 10
E-mail: infos@hamamatsu.fr

Swiss Office
Dornacherplatz 7, 4500 Solothurn, Switzerland
Telephone: (41)32 625 60 60, Fax: (41)32 625 60 61
E-mail: swiss@hamamatsu.ch

Belgian Office
Axisparc Technology, Rue André Dumont 7,
1435 Mont-Saint-Guibert, Belgium
Telephone: (32)10 45 63 34, Fax: (32)10 45 63 67
E-mail: info@hamamatsu.be

Spanish Office
C. Argenters 4, edif 2, Parque Tecnológico del Vallés,
08290 Cerdanyola, (Barcelona), Spain
Telephone: (34)93 582 44 30
E-mail: infospain@hamamatsu.es

North Europe and CIS:
HAMAMATSU PHOTONICS NORDEN AB
Main Office
Torshamnsgatan 35, 16440 Kista, Sweden
Telephone: (46)8-509-031-00, Fax: (46)8-509-031-01
E-mail: info@hamamatsu.se

Italy:
HAMAMATSU PHOTONICS ITALIA S.R.L.
Main Office
Strada della Moia, 1 int. 6 20044 Arese (Milano), Italy
Telephone: (39)02-93 58 17 33, Fax: (39)02-93 58 17 41
E-mail: info@hamamatsu.it

Rome Office
Viale Cesare Pavese, 435, 00144 Roma, Italy
Telephone: (39)06-50 51 34 54
E-mail: inforoma@hamamatsu.it

United Kingdom:
HAMAMATSU PHOTONICS UK LIMITED
Main Office
2 Howard Court, 10 Tewin Road, Welwyn Garden City,
Hertfordshire, AL7 1BW, UK
Telephone: (44)1707-294888, Fax: (44)1707-325777
E-mail: info@hamamatsu.co.uk

South Africa Contact:
9 Beukes Avenue, Highway Gardens, Edenvale,
1609, South Africa
Telephone/Fax: (27)11-609-0367

Impressum

Hamamatsu Photonics News

Publisher and copyright:
HAMAMATSU PHOTONICS K.K.
325-6, Sunayama-cho, Naka-ku, Hamamatsu City,
Shizuoka Pref., 430-8587, Japan
Telephone: (81)53 452 2141, Fax: (81)53 456 7889
http://www.hamamatsu.com
info@hamamatsu.eu

Editor and responsible for content:
Alexander Kirst

Publishing frequency:
Date of this issue
April 2023

Copies: 40000

Graphics and realisation:
SINNIQ GmbH
www.sinniq.com

Layout pictures:
Page 5, 6, 9: Shutterstock

Printing:
Mühlbauer Druck GmbH

Hamamatsu News – now also online:
www.hamamatsu-news.com

HAMAMATSU

PHOTON IS OUR BUSINESS

www.hamamatsu.com